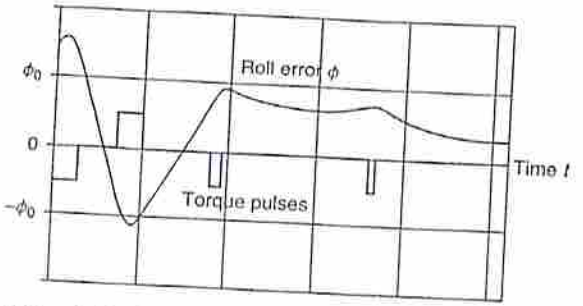

Figure 9.23 Roll error with full PID control, with a disturbance torque

As we have indicated, there are a number of limitations to the brief treatment presented here. For a text in which these are addressed in the context of spacecraft control, the reader is referred to Reference [3]. More generally, the topic of automatic control has a vast literature. Reference texts include [9] and [10], the latter being a brief and approachable text for those wishing to acquire the basics rapidly.

REFERENCES

[1] Wertz, J. R. (1978) *Spacecraft Attitude Determination and Control*, Kluwer, Dordrecht, The Netherlands.
[2] Hughes, P. C. (1985) *Spacecraft Attitude Dynamics*, John Wiley & Sons, New York.
[3] Sidi, M. J. (1997) *Spacecraft Dynamics and Control—A Practical Engineering Approach*, Cambridge University Press, New York.
[4] Fortescue, P. W. and Belo, E. M. (1989) Control decoupling analysis for gyroscopic effects in rolling missiles, *J. Guidance, Control Dynam.*, **12** (6), 798–805.
[5] Chu, Q. P. and van Woerkom, P. Th. L. M. (1997) GPS for low-cost attitude determination, IAF-97-A.2.03, 48th *International Astronautical Congress*, Turin.
[6] Bryan, G. H. (1890) On the beats in the vibrations of a revolving cylinder or bell, *Proceedings of the Cambridge Philosophical Society*, Vol. 7, pp. 101–111.
[7] Fujishima, S., Nakamura, T. and Fujimoto, K. (1991) Piezoelectric Vibratory Gyroscope Using Flexural Vibration of a Triangular Bar, 45th *Annual Symposium on Frequency Control*, pp. 261–265.
[8] Gelb, A. (1974) *Applied Optimal Estimation*, MIT Press, Cambridge, MA.
[9] Nise, N. S. (2000) *Control Systems Engineering* (3rd edn), John Wiley & Sons, New York.
[10] Schwarzenbach, J. (1996) *Essentials of Control*, Longman, UK.

10 ELECTRICAL POWER SYSTEMS

John P. W. Stark

Department of Engineering, Queen Mary, University of London

10.1 INTRODUCTION

Provision of electrical power for space vehicles is, perhaps, the most fundamental requirement for the satellite payload. Power-system failure necessarily results in the loss of a space mission, and it is interesting to note that many of the early satellite systems failed due to such a loss. The demand for power has increased and is characterized by enhanced spacecraft operational complexity and sophistication. The earliest spacecraft, such as Vanguard 1, typically required a power raising capability of only ~1 W, whereas current communications satellites typically require three orders of magnitude greater than this. Evolving trends suggest that a further two orders of magnitude may still be needed. However, prediction of future power demand must always be treated with a great deal of caution. In the early 1980s there was great focus upon large systems, particularly with the infrastructure elements associated with space stations, containing both manned and unmanned elements. The potential for Solar Power Satellite systems (SPS), large orbiting power stations generating GW of electrical power for terrestrial use, was investigated in many studies, initially supported in the United States of America by both NASA and DoE, and in Europe by the European Space Agency (ESA) [1]. Political and technical issues have slowed down such developments, and large is no longer necessarily more beautiful. Manned systems do require higher power levels, perhaps of the order of 300 kW. Commercial communication services and broadcast systems are still seeing a slowly evolving trend to higher power levels, but enhanced system performance is reducing power demands. However, much focus is now also upon smaller satellite systems (see Chapter 18) where cost and system efficiency are critical system drivers.

The best methods of raising power can be broadly related to power level and mission time as shown in Figure 10.1. It is apparent that photovoltaic (solar cells) or radioisotope thermoelectric generators (RTGs) are appropriate for the power requirements typical of present generation spacecraft, namely, a few kilowatts for missions of several years. For shorter periods, fuel cells are advantageous, and for periods of less than a few days

Spacecraft Systems Engineering (Third Edition). Edited by P. W. Fortescue, J. P. W. Stark and G. G. Swinerd

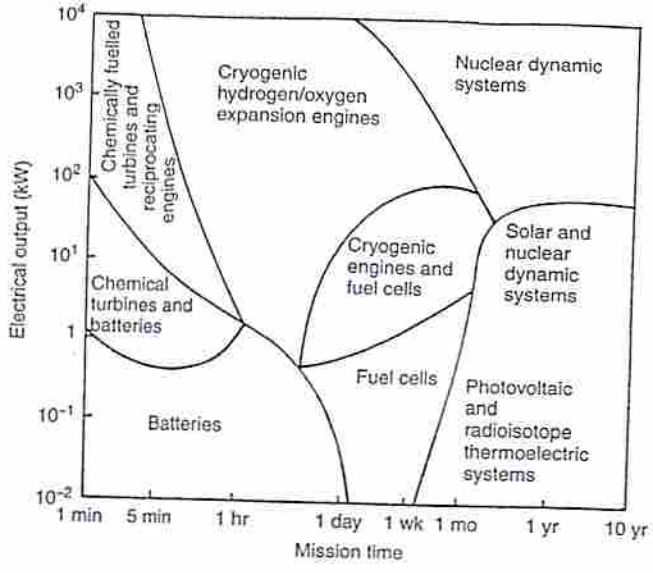

Figure 10.1 Power outputs: mission duration relationship between energy source and appropriate operational scenario [2] (From Angrist, S. W. (1982) *Direct Energy Conversion*, 4th edn, Copyright Allyn and Bacon, New York)

batteries come to the fore. It is not surprising, therefore, to discover that batteries are used in launch vehicles to provide the primary energy source, fuel cells are used in the Shuttle and both photovoltaic devices and RTG are used for general spacecraft operation, dependent upon the mission. It should be noted that nuclear sources of power such as RTG and nuclear dynamic systems are used for military applications, but are not generally acceptable for civilian vehicles in Earth orbit. Indeed, during the 1990s, an increasing public awareness of environmental issues resulted in protests concerning the launch of nuclear-based sources for scientific purposes—for example, the launch of the Cassini–Huygens mission. Before the individual elements of a spacecraft power system are considered, the overall power system configuration will be described briefly.

10.2 POWER SYSTEM ELEMENTS

In general a spacecraft power system consists of three main elements: primary and secondary energy sources, and a power control/distribution network. These are shown schematically in Figure 10.2.

The *primary energy source* converts a fuel into electrical power. On early space flights and on launch vehicles, batteries have provided this. Strictly these systems do not have a fuel element, in that a battery is a device that stores energy rather than performing a direct energy conversion process.

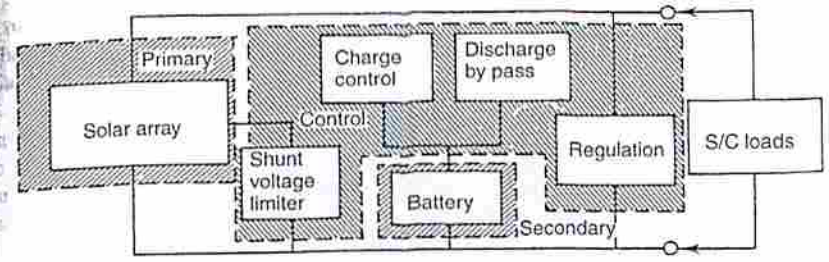

Figure 10.2 Schematic of typical spacecraft power system block elements

The majority of present-day spacecraft use a solar array as the primary energy source. The 'fuel' in this case is solar radiant energy, which is converted *via* the photovoltaic effect (see Section 10.3.1) into electrical energy. On manned missions of short duration, fuel cells have been used most frequently as the primary source; for longer duration flights associated with space stations such as Mir and ISS, the combination of solar arrays and fuel cells has been adopted. These electrochemical devices perform a controlled chemical reaction, in such a way that electrical energy may be derived rather than heat energy. The fuels used for space operation are hydrogen and oxygen yielding water as the reaction product: this may then be drunk by astronauts. Nuclear systems utilize either a radioactive decay process (RTG uses this) or a nuclear fission process as the energy source. RTG makes use of the thermoelectric effect, whereas fission reactors operate in a manner similar to terrestrial nuclear power plants [3].

The *secondary energy source* is required to store energy and subsequently deliver electrical power to the satellite system and its payload, when the primary system's energy is not available. The most usual situation when this condition arises is during an eclipse period when the primary system is a solar array. The eclipse's duration depends on the spacecraft orbit (see Section 5.3.2 of Chapter 5). Typically for Low Earth Orbit (LEO), a 35-minute eclipse occurs in each orbit for low-inclination satellites: in Geostationary Earth orbit (GEO), eclipses occur only during equinoctial periods, with a maximum duration of 1.2 h in a 24-hour period. For such short times, batteries demonstrate the highest efficiency. However, for systems that require high-power levels, typically 100 kW, a solar array/regenerative fuel–cell combination has improved characteristics over a solar array/battery combination. Regenerative fuel cells operate in a closed fuel cycle: H_2/O_2 fuel is consumed to form water on the 'discharge' cycle and electrolysis of water is performed during the 'charge' cycle, with power for this being derived from the solar array [4]. Whilst the net efficiency is low, only 50 to 60% compared to nearly 90% for a battery, it is possible by judicious sizing of the fuel (H_2/O_2) component to reduce the size of the solar array required for primary power raising. For LEO operations in which aerodynamic drag is significant, the reduction in array area reduces the mass of propellant required for orbit control leading to a lower wet mass of the system at launch compared with the conventional array/battery configuration.

The *power control and distribution network* is required to deliver appropriate voltage–current levels to all spacecraft loads when required. Several salient features should be noted.

The primary power source always degrades during the mission. Thus, at its start an excess of power will be generated, and it is necessary to provide an ancillary load to dissipate it. The simplest way to do this is to use a resistive load, generally external to the main spacecraft structure in order to simplify the thermal design.

Both primary and secondary power system characteristics will change during the mission, leading to a requirement for voltage and/or current regulation. The changes arise due to both degradation effects, such as cell failures, and also illumination variations caused by changing solar array aspect angles with respect to the Sun. The customary approach is to use a voltage shunt regulator across the array.

Charge control of a battery system is particularly important to maintain the lifetime and reliability of battery units. It generally necessitates both current and voltage control. A variety of techniques may be used to sample the state of a battery and these will be discussed in Section 10.5. Discharge control is also required in order to limit current output.

10.3 PRIMARY POWER SYSTEMS

10.3.1 Solar arrays

A solar array is an assembly of many thousand individual solar cells, connected in a suitable way to provide dc power levels from a few watts to tens of kilowatts. For a detailed description of both terrestrial and space solar arrays, Rauschenbach [5] is recommended.

Each *solar cell* assembly has a semiconductor $p-n$ junction as shown schematically in Figure 10.3. For spacecraft applications, the base material typically has a resistivity of between 10^{-3} and $10^{2}\,\Omega\,\text{cm}$. Using silicon, for example, it might be doped with boron to form the p-type material (electron deficient), and with phosphorous for the n-type material (electron excess).

With no illumination, the junction achieves an equilibrium state in which no current flows. But when it is illuminated with suitable radiation, photons with sufficient energy will create electron–hole pairs, and the radiation is converted to a potential across the cell with usable electrical power. The incident photon energy needed for this must exceed a *band gap* that depends upon the material, as shown in Table 10.1. Photons with excess energy dissipate it as heat within the cell, leading to reduced efficiency.

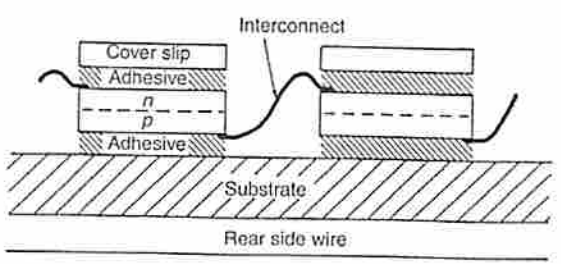

Figure 10.3 Schematic of a typical solar cell assembly

Table 10.1 Properties of semiconductor materials

Material	Band gap (eV)	Maximum wavelength (μm)
Si	1.12	1.12
CdS	1.2	1.03
GaAs	1.35	0.92
GaP	2.24	0.554
CdTe	2.1	0.59

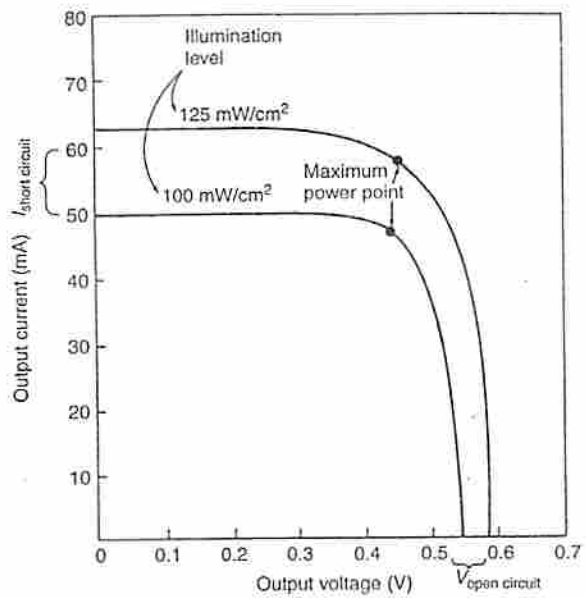

Figure 10.4 Current–voltage characteristic for a typical solar cell. The short-circuit current is dependent upon both the illumination level and the size (area) of the cell (From Angrist, S. W. (1982) *Direct Energy Conversion*, 4th edn, Copyright Allyn and Bacon, New York)

Characteristic voltage-current curves for cells are shown in Figure 10.4. Typically open-circuit voltages for silicon cells lie between 0.5 and 0.6 V under solar illumination. The plot of power against voltage (Figure 10.5) has a clear maximum, with a particularly rapid fall once the optimum voltage is exceeded. On some spacecraft maximum-power-point tracking is used to operate the array most efficiently. Increase in cell temperature results in decreasing open-circuit voltage with only a modest increase in short-circuit current. The theoretical maximum efficiency of both silicon (Si) and gallium arsenide (GaAs) cells

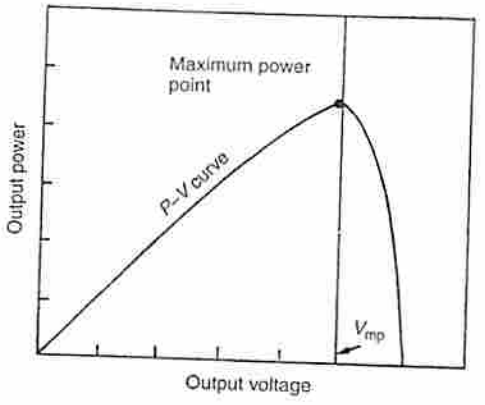

Figure 10.5 Power–voltage characteristic for a typical solar cell (From *Solar cell array design handbook* by Rauschenbach, H. S. Copyright © 1980 by Van Nostrand Reinhold. All rights reserved)

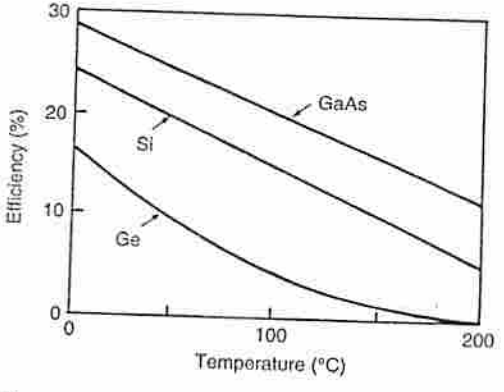

Figure 10.6 Theoretical cell efficiency as a function of temperature for three semiconductor materials (From *Solar Cell Array Design Handbook* by Rauschenbach, H. S. Copyright © 1980 by Van Nostrand Reinhold. All rights reserved)

is shown as a function of temperature in Figure 10.6. It shows the particular sensitivity of Si to temperature and also the improved performance of GaAs at high temperatures. This means that it is theoretically possible to use a focusing optical arrangement for GaAs cells such that these cells may be illuminated by an intensity greater than the nominal radiation intensity of 1.4 kW/m^2 in Earth orbit. Fewer cells would then be required to provide a given power level, which could result in array cost reductions since the cell cost is a large proportion of the total cost. Concentration ratios as high as 100 : 1 for GaAs cells have been investigated in such studies, but at present the benefits of these systems are not conclusive. The majority of commercial satellites, together with ISS have utilized silicon for solar cells. Perhaps two of the most notable civilian uses for GaAs have been on the Mir space station and the satellites used in the Iridium constellation.

The *n-type contact* on the upper surface of the cell is in the form of a multiple-finger arrangement. These fingers are required for efficient current collection, whilst maintaining good optical transparency (typically ~60%). They are connected at a bar, along one edge of the cell. Frequently titanium/silver (Ti/Ag) is used for this.

Radiation damage is a problem with solar cells. In general, Si cells having higher base resistivity (~10 Ω cm) are the most tolerant of radiation. Furthermore, cells have the *n*-type material uppermost, since on early space flights it was discovered that cells having the *p*-type material as the upper region rapidly suffered from radiation damage. Thin cells suffer less than thicker ones, but at present they have a lower conversion efficiency. GaAs cells are more radiation tolerant than Si and for this reason there is considerable interest and effort in their development.

The *cover glass* provides environmental and radiation protection. For design purposes, the particle fluence of a spacecraft's radiation environment may be expressed as an equivalent fluence of monoenergetic 1 MeV electrons (see Figure 10.7). Degradation of cell output to this irradiation is generally available from manufacturers' data; Figure 10.8 shows typical degradation curves for cells with a variety of thicknesses.

The effectiveness of the cover glass depends on its density and thickness. Suitable glass microsheet is commercially available in several thicknesses from 50 μm to 500 μm [6]. Their absorption of radiation follows approximately an exponential law, so that the intensity of radiation after traversing a depth x into the glass is

$$I \sim I_0 e^{-k\rho x} \tag{10.1}$$

where I_0 is the initial radiation fluence at $x = 0$, ρ is the density of material and k is an energy-dependent absorption coefficient. For fused silica, Figure 10.9 shows the effect of changing glass thickness. It should be noted that in order to evaluate the total radiation fluence absorbed by the solar cell, both front-side and rear-side fluences must be calculated. On rigid panel arrays mounted on honeycomb structure, and on solar arrays bonded to the spacecraft wall (e.g. spinning spacecraft) the rear side is effectively screened from radiation, whilst on lightweight arrays this is not the case. Using the data supplied in Figures 10.7 to 10.9, it is possible to derive the area of active solar cells required to meet a specific mission requirement of end of life (EOL) performance. Suppose that an output of 1 kW is required at EOL for a satellite in a circular, equatorial orbit at 1000 km altitude. Assume that the cell to be used is made of silicon, 150 μm thick, having the properties shown in Figure 10.8. The mission duration is to be 5 years. Note that in the discussion that follows, the numerical values are approximate.

The starting point is to use Figure 10.7 to find the total damage equivalent 1 MeV electron fluence for a cell protected by a 150 μm cover slip. At 1000 km, this Figure shows that the damage equivalent due to protons is 1.7×10^{14} electrons/cm/year and that due to electrons is 2×10^{12} electrons/cm/year. The total flux in 5 years is therefore $5(1.72 \times 10^{14})$ electrons/cm/year, or 8.6×10^{14} electrons/cm/year. It is evident that the damage due to protons is much greater than that from electrons, as noted in Section 2.3

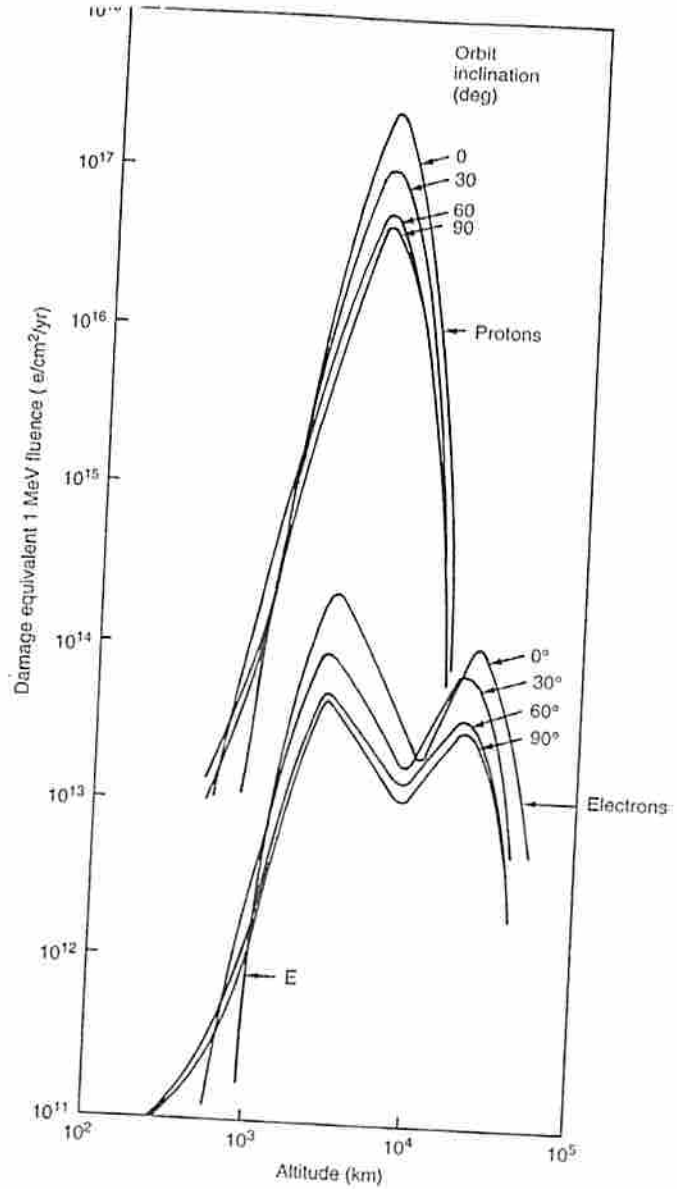

Figure 10.7 Damage equivalent 1 MeV fluence caused by electrons and protons due to trapped particles, to silicon cells protected by 150 μm fused silica covers and infinitely thick rear shielding [5] (From *Solar cell array design handbook* by Rauschenbach, H. S. Copyright © 1980 by Van Nostrand Reinhold. All rights reserved)

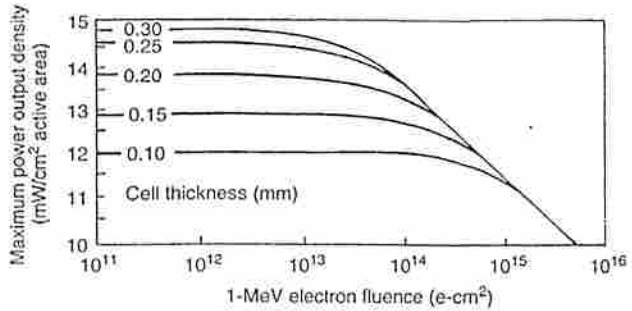

Figure 10.8 Effects of thickness and fluence on conventional non-p^+ silicon solar cell performance [5] (From *Solar Cell Array Design Handbook* by Rauschenbach, H. S. Copyright © 1980 Van Nostrand Reinhold. All rights reserved)

of Chapter 2. From Figure 10.8, the power per unit area is 11.5 mW/cm^2. It is however, noticeable from this Figure that a significant deterioration in the performance of the cell is evident at such a high radiation dose. A reduction in dose may be achieved by increasing the cover slip thickness. For example, if a cover slip of 500 μm were to be used, then the flux will be reduced according to the data presented in Figure 10.9 by a factor of 0.6. Thus the expected radiation dose absorbed in the cell after 5 years would then only be 5.2×10^{14} electrons/cm, yielding an EOL performance of 12 mW/cm^2, an improvement of approximately 4%. The mass increase associated with the use of this cover slip, assuming as a first approximation that the density of the cover slip is the same as that of the cell, will be (mass of 500 μm cover slip plus 150 μm cell)/(mass of 150 μm cover slip plus 150 μm cell), equivalent to a factor of nearly 2.2. This increase in mass needs to be considered however alongside the cost increase associated with the alternative of a 4% increase in the number of cells. The thinner cover slips result in an active area of (1000/0.0115) cm^2, or 8.7 m^2, whilst the thicker protection requires an area of only 8.3 m^2.

Additional features required of the cover glass are that it provides good optical coupling between free space and glass and also between glass and adhesive, and that it provides suitable wavelength selection, limiting the UV flux to the adhesive layer and the cell. These features are achieved using an anti-reflection coating, such as magnesium fluoride on the upper surface, perhaps with an additional indium oxide conductive coating as described in Chapter 2. A UV-filter coating may be applied to the underside of the cell, to reflect UV radiation. For a cover glass with cerium doping, additional UV filtering is unnecessary.

For *efficient cell operation* and insensitivity to radiation, a shallow junction depth (typically less than 10 μm) is required. Various Si cell configurations have been investigated to improve conversion efficiency. These include the following:

- Back-surface reflectors (BSRs), used, for example, on Spot and Orion, to reflect unabsorbed radiation from the rear side of the (p)-region back through the cell. This reduces cell heating.

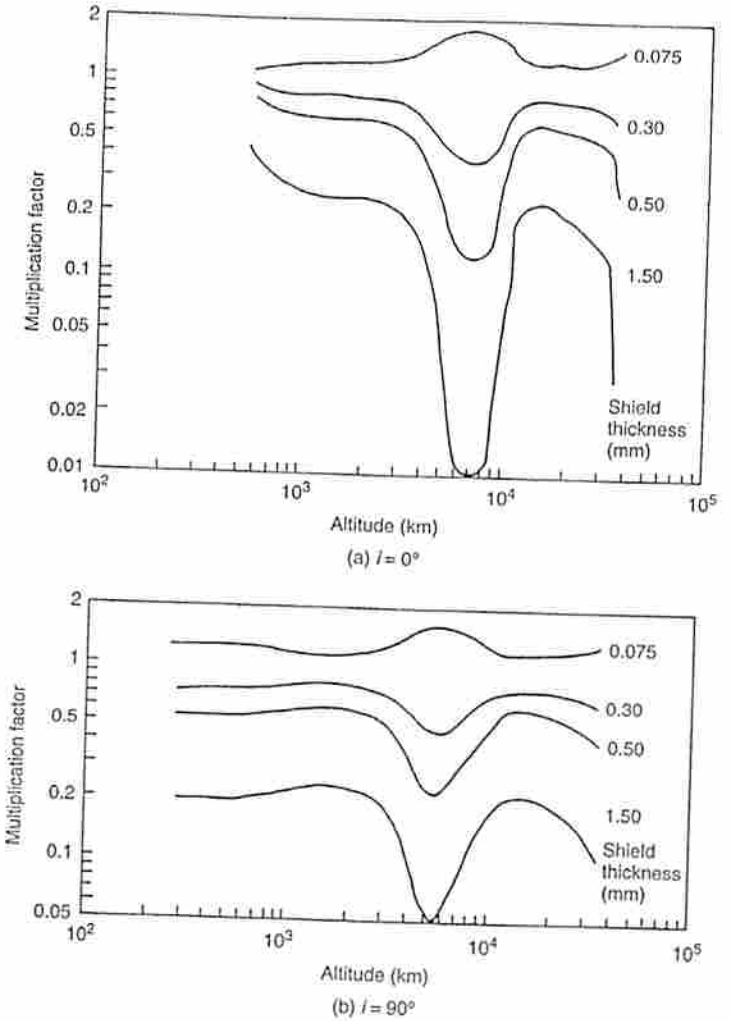

Figure 10.9 Multiplicative factors to be applied to damage fluence on a solar cell as a function of cover slip (shield) thickness, and operational orbit height (From *Solar Array Design Handbook* by Rauschenbach, H. S. Copyright © 1980 Van Nostrand Reinhold. All rights reserved)

- The introduction of a p^+-region or back-surface field (BSF) at the rear of the *p*-regions. This exhibits higher output due to enhanced carrier collection efficiency, but the improvement is lost under high fluence damage. This technology has been used on the array for the Hubble Space Telescope (HST) and Envisat.
- The use of a textured front surface of the cell reduces reflection from the cell surface.

Solar arrays using Si cells are made from individual cells that at present are generally rectangular, 2 cm × 4 cm, having a conversion efficiency of ~12 to 14%. To improve packing efficiency, much work on high-efficiency 5 cm × 5 cm cells is under way. The cells have a thickness of between 50 and 250 μm, ~200 μm being used for the majority of arrays. Silicon cells having a thickness of 50 μm are now able to convert with a power density of 120 W/m^2; thinner GaAs cells ~5 μm with an efficiency of 21% have also been developed, but are not available for space systems at the time of writing.

Interconnections between cells represent a major array failure hazard. This arises because of the thermal cycling inherent upon entry/departure from sunlight to eclipse. Since the materials used for cell and substrate are different, differential expansion takes place during the rapid temperature change (~100 °C in a few minutes). Thermal stress-relieving loops are required to reduce such failure mechanisms as interconnect lift-off and fracture.

Atomic oxygen effects on exposed interconnects have been mentioned earlier, in Chapter 2. A particular problem of the solar cell interconnection is that historically these have always been made of thin silver foil. Silver has a high capture efficiency for atomic oxygen, resulting in the formation of a variety of silver oxides. The process results in thinning due to flake-off of the oxides and hence an increase in interconnection resistivity. This leads to a loss of power. In the case of the HST array, the interconnects were originally designed to be pure silver. The delay in the original launch date (because of the Challenger accident) permitted a redesign in which silver was used only as a surface layer on a molybdenum interconnect. During flight, the silver eroded revealing the molybdenum, which is oxidation resistant. The power output from the array has thus been maintained at the predicted value for the life of the mission.

A variety of *substrate materials* have been used and proven in space. Frequently Kapton with glass- or carbon- fibre reinforcement, ~100 μm thick, forms the immediate interface with the cell, which may be mounted on a honeycomb panel for rigidity (e.g. Tracking and Data Relay Satellite (TDRS) solar array). Flexible cell blankets have also been used to reduce mass. The HST solar array is a typical example, with glass fibre reinforcing the Kapton. In general, for the largest arrays, flexible substrate materials offer mass savings. But it is interesting to note that early work [7] has shown that for power levels up to 6 kW, mass savings occur when using advanced rigid arrays, wherein Kapton is reinforced with carbon fibre. Fokker Space has continued the development of advanced rigid solar arrays using both Si and GaAs, with in-orbit power (beginning of life (BOL)) in excess of 8 kW [8].

As noted earlier, individual cells produce power at a voltage of ~0.5 V, and it is necessary to connect many cells in series. Reliability is then achieved by additional parallel coupling at each cell; typically three or four cells form a parallel combination. This series–parallel arrangement is called a *solar cell string*. Further protection is afforded using shunt diodes that provide current bypass paths should individual cells become shadowed. Shadowing can cause cell failures since if a cell is unable to generate power because of loss of illumination, then the entire string voltage may appear as a reverse bias voltage across the cell.

System level interactions

Now consider the *system level interactions* between the solar array design and the vehicle itself. The relatively low conversion efficiency of an array results in the need for large

areas of solar cells to intercept sufficient solar radiation for the power demand. Examples of typical array configurations, associated with generic stabilization types are illustrated in Chapter 9.

For a spinning satellite, using either dual spin or simple spin ACS, the 'drum' size evidently limits the power that can be generated. The drum itself is limited by the launch volume. A possible solution is to introduce an additional mechanism such as the 'drop skirt' as used on Intelsat VI, where a larger-diameter hollow cylinder is deployed to expose additional cell area. Thruster plume impingement in such a configuration can, however, cause both disturbance torques and contamination.

Other aspects to note for the spinning satellite solar array are coupled with the thermal environment. Assuming a typical spin rate of ~50 rpm, the average temperature of the array can be maintained at a lower value than for the three-axis configuration. This leads to an increased efficiency of the individual cells, and thus a decrease in the required active cell area. However, since not all the array is instantaneously illuminated, a factor of $\sim\pi$ times the number of cells is required for the same collected power. Since also on the spinner, the array is mounted essentially on the body of the spacecraft, the temperature excursions noted on the array (between sunlit and eclipse phases) are reduced, having a significant impact on reducing the thermal shock characteristic of a three-axis deployed solar array.

Considering the three-axis-stabilized satellite, the solar array requires a mechanism to deploy the stowed array following launch and then orientate it appropriately to track the Sun. These deployment mechanisms may be of a simple extending telescopic construction, or of the 'Coilable' variety. (See Chapter 15). In the Astromast, the carbon-fibre members of the mast are deformed by coiling them into a stowage container. They may then be driven out by a screw mechanism to the underformed (extended) configuration.

Tensioning wires are then required to achieve an acceptable minimum fundamental frequency of the array largely because of AOCS requirements. On three-axis-stabilized vehicles, power take-off from the array generally, but not always, requires a rotary degree of freedom between the satellite and the array, in order that pointing requirements of the array and the payload may be met. This requires two elements—the mechanical rotation device to allow the body to move relative to the array (with appropriate sensing systems) and an electrical power take-off device. (See Chapter 15) The provision of power using a solar array clearly has many design interactions with the rest of the spacecraft system.

Table 10.2 summarizes performance characteristics for several solar arrays. A method for array sizing is given in Section 10.6.

Table 10.2 Solar array performance figures

Array	Type	BOL power (kW)	Specific mass (W/kg)	Power density (W/m²)
XMM	Rigid	2.5	32	215
Astra 2B	Rigid	9.2	52	409
Comets	Flexible	6.3	34	146

Note: XMM: X-ray multi-mirror mission.

10.3.2 Fuel cells

Fuel cells provide the primary power source for the Shuttle orbiter. Originally they were designed as part of the Mercury, Gemini and Apollo US manned missions. Table 10.3 shows how their performance has evolved since the earliest days of manned space flight. A fuel cell converts the chemical energy of an oxidation reaction directly into electrical energy, with minimal thermal changes. From a system viewpoint, a major advantage is its flexibility. For example, it provides power during both sunlit and eclipse periods, and the fuel has a high-energy density and thus provides a compact solution compared with a solar array. The evident disadvantage is the need to carry fuel.

The *hydrogen/oxygen fuel cell* has been used for space applications, a product of the reaction being water. This is clearly useful for manned missions. A schematic diagram of such a cell is shown in Figure 10.10. This technology has also been proposed for lunar rover missions [9].

The voltage that appears at the terminals of an ideal cell is given by

$$E_r = \frac{-\Delta G}{nF} \tag{10.2}$$

where ΔG is the change of Gibbs free energy occurring in the reaction, n is the number of electrons transferred and F is the Faraday constant (product of Avogadro number and elementary charge) equal to 9.65×10^4 C/mol. For the reaction of the H_2/O_2 cell, two electrons are transferred per mole of water formed and ΔG has the value of -237.2 kJ/mole at 25 °C. The reaction takes place spontaneously.

Thus the reversible voltage of the ideal cell is $237.2 \times 10^3/(2 \times 9.65 \times 10^4) = 1.229$ V.

In practice this is not realized because there are various irreversibilities, termed polarization losses. Figure 10.11 shows a typical current–voltage curve for a hydrogen/oxygen fuel cell. Initially, as soon as a current is drawn from the cell, a rapid drop in voltage occurs. This is associated with the energy required to activate the electrode reactions. For the H_2/O_2 fuel cell these are three-phase: gas (fuel), solid (electrode) and liquid (electrolyte—this can also be a solid). It is necessary for the reactants to be chemisorbed onto the electrode, a process that requires breaking and forming new chemical bonds, and requires energy; hence the voltage drops. The process is called activation polarization.

Table 10.3 Performance summary of fuel cells for space use

System	Specific power (W/kg)	Operation
Gemini	33	
Apollo	25	
Shuttle	275	2500 h at P_{ave}
SPE technology	110–146	>40 000 h
Alkaline technology	367	>3000 h
Alkaline technology	110	>40 000 h
Goal (lightweight cell)	550	

Note: SPE solid polymer electrolyte.

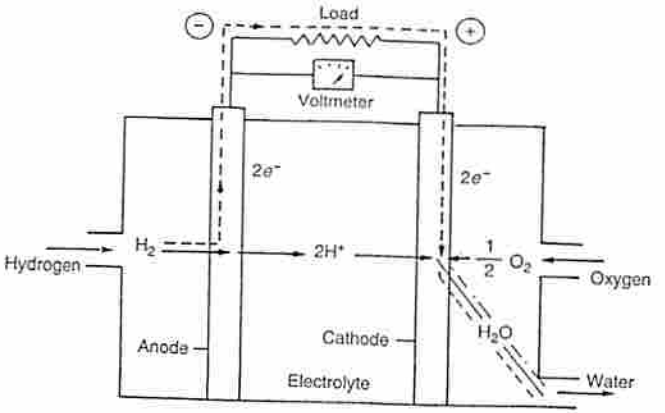

Figure 10.10 Schematic of a hydrogen/oxygen fuel cell. At the anode–electrolyte interface, hydrogen dissociates into hydrogen ions and electrons. The hydrogen ions migrate through the electrolyte to the cathode interface where they combine with the electrons that have traversed the load [2] (From Angrist, S. W. (1982) *Direct Energy Conversion*, 4th edn, Copyright Allyn and Bacon, New York)

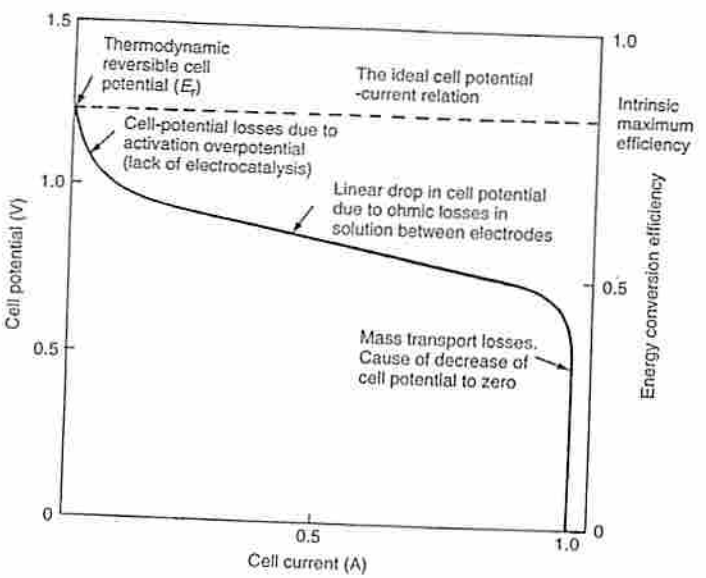

Figure 10.11 Typical cell potential and efficiency–current relation of an electrochemical electricity producer showing regions of major influence of various types of overpotential losses (Source [10])

The magnitude of voltage drop is given by the Tafel equation:

$$\Delta V_{ACT} = a + b \ln J \tag{10.3}$$

where J is the current density at the electrodes, and a and b are temperature-dependent constants for the reaction/surface description.

As the current drawn increases, a linear voltage–current relation is noted. This is simply because of the resistive nature of the electrolyte.

At high current values problems arise because of the transport of reactants to the reaction sites, a feature that is particularly important at porous electrodes since pressure gradients are set up that limit flow rates. Additionally, species concentrations are not uniform and thus ionic species can create a back emf. This concentration polarization provides the ultimate limit on current density that may be achieved by a fuel cell. All of these electrochemical polarization processes are common to both batteries and fuel cells, and their voltage–current characteristics are very similar.

Early fuel-cell systems were primarily based upon the technology of solid polymer electrolyte (SPE). For the Gemini series, 1 kW was produced at a specific power of 33 W/kg, within a volume of 0.05 m^3, and the objective to extend missions to greater than four days was achieved. However, the water produced was not of drinking quality because of degradation of the fuel-cell membrane.

The Apollo system, also used for Skylab, was based upon matrix aqueous alkaline technology and achieved a power level of 1.5 kW at a specific power of 25 W/kg. It had to operate whilst the vehicle was on the lunar surface, at a temperature greater than 394 K. The selected system, a Bacon fuel cell, operated at 505 K.

Shuttle developments, also based upon the alkaline technology, have improved the specific power by an order of magnitude, ~12 kW, 275 W/kg. Further, the start-up time for this cell is 15 min with shutdown being instantaneous, whereas for Apollo, 24-hour start-up periods were required with 17-hour shutdown. Table 10.3 summarizes past and present fuel-cell status. Regenerative fuel cells wherein water is also electrolysed are not yet space-proven.

10.3.3 Radioisotope thermoelectric generators (RTG)

For deep-space missions, the use of fuel cells is precluded by their long duration. Solar arrays produce less power as they move away from the Sun, by a factor of approximately $(r_E/r_{S/C})^{1.5}$, where $r_{S/C}$ and r_E are the distances from the Sun to the spacecraft and to the Earth respectively. This factor comes about from the combined effect of the reduction in the intensity of the illumination from the Sun as the spacecraft moves away from it, partly offset by the beneficial effect of the reduction in the temperature of the solar cells.

For spacecraft travelling further than Mars, solar arrays show disadvantages from a system viewpoint, compared with radioisotope generators.

The operation of a RTG is based on the thermoelectric effect noted by Seebeck, that it is possible to generate a voltage between two materials, A and B (either conductors or semiconductors) if a temperature difference is maintained (see Figure 10.12). This is analogous to a thermocouple. Practical RTG space systems utilize two semiconductor materials—one p-type, the other n-type—in order to exploit the effect.

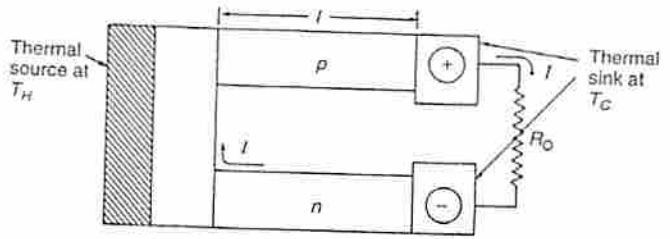

Figure 10.12 Schematic diagram of a semiconductor radioisotope generator (From Angrist, S. W. (1982) *Direct energy conversion*, 4th edn, Copyright Allyn and Bacon, New York)

The power output from such a device is a function of the absolute temperature of the hot junction, the temperature difference that may be maintained between the junctions and also the properties of the materials. Because such devices are relatively inefficient (less than 10%), one major problem in their design is removing waste heat.

The heat source used in space systems is derived from the spontaneous decay of a radioactive material. As this decays, it emits high-energy particles that can lose part of their energy in heating absorbing materials. Suitable fuels are listed in Table 10.4, and shows the half-life ($\tau_{1/2}$) for each of the fuels, namely, the time required for the amount of a given radioactive isotope in a sample to halve. Thus over a period of time t, the power available from such a fuel decreases by an amount given by

$$P_t = P_0 \exp\left(\frac{-0.693}{\tau_{1/2}} t\right) \tag{10.4}$$

where P_t is the power at time t after some initial time t_0.

Table 10.4 indicates that high specific power levels are available from sources with shorter half-lives (and hence shorter duration missions). For deep-space missions a long life isotope is essential; for example, the design life for the Cassini–Saturn orbiter is 11 years, after which time the electrical power source is required to be 628 W. For these missions Plutonium is used exclusively.

Table 10.4 Possible fuels and their performance for radioisotope generators (From Angrist, S. W. (1982) *Direct energy conversion*, 4th edn, Copyright Allyn and Bacon, New York)

Isotope	Fuel form	Decay	Power density (W/g)	$\tau_{1/2}$(yr)
Polonium 210	GdPo	α	82	0.38
Plutonium 238	PuO_2	α	0.41	86.4
Curium 242	Cm_2O_3	α	98	0.4
Strontium 90	SrO	β	0.24	28.0

The advantages of RTGs over other systems include the following:

1. They provide independence of power production from spacecraft orientation and shadowing.
2. They provide independence of distance from the Sun (deep-space missions are possible).
3. They can provide low power levels for long periods of time.
4. They are not susceptible to radiation damage in the Van Allen belts.
5. They are suitable for missions with long eclipse periods, for example, lunar landers.

The disadvantages of RTG systems need also be considered, and include

1. They adversely affect the radiation environment of the satellite whilst in orbit. This will influence the spacecraft configuration significantly as may be seen from Figure 10.13, which shows the Galileo spacecraft. In this instance, the RTG needs to be deployed on a lengthy boom away from the main satellite bus.
2. Careful handling procedures are required during satellite integration owing to the radiation hazard posed by the radioactive source.
3. High temperature operation is required for efficient energy conversion. This impacts upon the thermal environment of the vehicle, and again on vehicle configuration.
4. RTGs are a source of interference for plasma diagnostic equipment that may be carried as part of the scientific objectives of the mission.
5. At the political level there has been increasing concern expressed at the inclusion of radioactive material on board a satellite. This is principally of concern because of the potential for such a source to be dispersed in the atmosphere, should there be a launch failure.

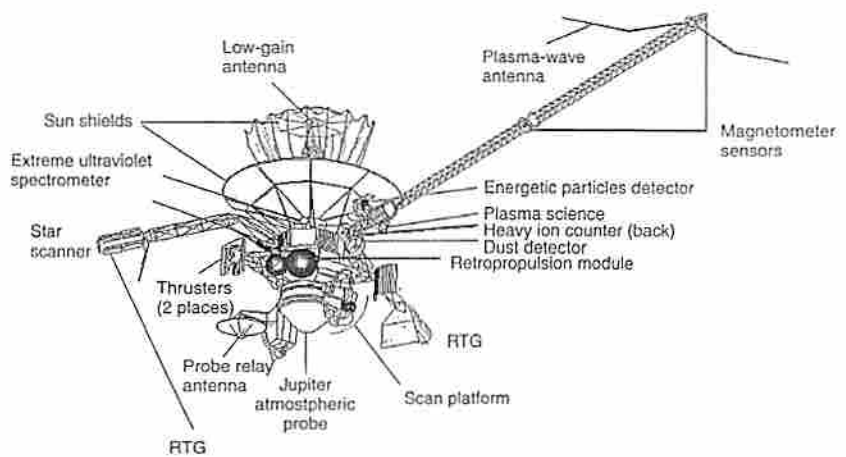

Figure 10.13 The Galileo spacecraft configuration, showing the position of the RTG sources (Courtesy of NASA/JPL/Caltech)

Table 10.5 RTG system performance

Name	Power (W)	kg/kW
Cassini (1997 launch)	628	195
Galileo probe/Ulysses (GPHS RTG, late 1980s)	285	195
Nimbus/Viking/Pioneer (SNAP 19, mid 1970s)	35	457
Apollo lunar surface experiment:		
SNAP-27, early 1970s	25	490
SNAP 9A, 1960s	73	261

System for Nuclear Auxiliary Power (SNAP-19), which powered the Viking lander vehicle to Mars, had a specific power of 2.2 W/kg, with a thermal/electric efficiency of ~5%. The output electrical power was 35 W. Table 10.5 summarizes data on RTG systems.

10.3.4 Other primary power systems

Two other primary power systems have been developed for operation—nuclear fission and solar heat. The former has been extensively used in the former Soviet space programme for military purposes. The latter has not flown in space yet, but a substantial effort has taken place in recent years in developing such systems for potential use on the International Space Station.

Nuclear fission systems

These systems operate in a similar way to conventional ground-based nuclear power stations, in that fissile material such as uranium-235 is used as a heat source. In space systems, this is used to drive a thermoelectric converter as noted in the preceding section. Specific features of space-based systems relate to the fail-safe requirement, particularly during launch.

Whilst the USA has invested substantially in the SNAP systems (even number SNAP designates a reactor system), these have not been used regularly. The main focus of their activity in recent years has been on the SP100 system [11]. It is notable, however, that the purchase of Russian technology by the US suggests that this US programme may not be pursued vigorously in the future.

Solar heat systems

The use of solar energy directly in the form of heat can provide system advantages. The heat energy can be used to drive a heat engine and then a rotary converter to electricity (solar dynamic), or directly be used as a heat source for a thermoelectric converter (solar thermoelectric).

Solar dynamic systems have had the greatest concentration of effort for the ISS. Design studies show that their end-to-end conversion efficiency is approximately 25% greater than for photovoltaics. This results in a reduced need for deployed collection area by

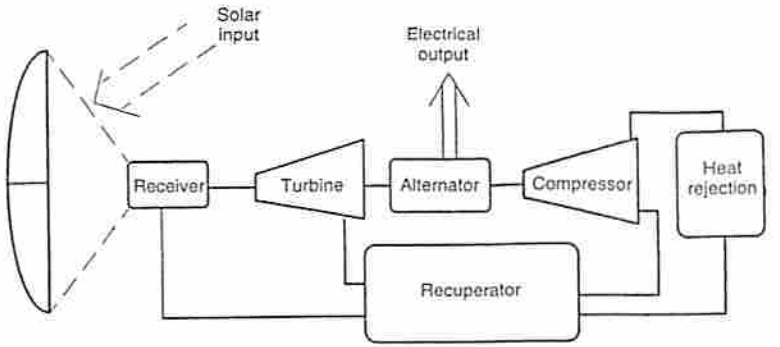

Figure 10.14 Solar dynamic Brayton cycle

about 25%, and consequently in reduced aerodynamic drag for LEO satellites. In the original concept for the ISS, primary power for the initial in-orbit capability was to be 75 kW, derived from photovoltaics. Power expansion was then assumed to be provided by solar dynamics in two units of 25 kW.

Solar dynamic systems, resulting in less drag, lead to lower fuel usage for orbit maintenance. This reduces the cost of station operation, principally by reducing the demand for Shuttle refuelling flights. An additional cost benefit arises from the lower maintenance costs envisaged for solar dynamic systems compared with photovoltaic systems. Over the lifetime of the Space Station, cost savings of several billions of dollars have been identified [12].

The concept studied by NASA, and which was the original baseline for the ISS solar dynamic system, is based upon the Brayton Cycle engine [12]. A block diagram of this is shown in Figure 10.14. The working fluid for this all-gas phase cycle is helium and xenon in such a proportion that the equivalent molecular weight is 40. This all-gas phase cycle minimizes problems of handling wet vapours (leading to erosion) and gravitational effects in transporting fluids. Storage of power within the concept was to be performed thermally, using the latent heat of fusion for a lithium fluoride/calcium fluoride mixture. This phase change occurs at 1042 K. Storing power in this way provides mass savings compared to battery technology, because of the high quality (temperature) heat energy.

Funding problems for the ISS have led to a cancellation of the power extension requirements. This has resulted in the cessation of most technology development work in this field. In the longer term, however, it is apparent from the activities that have been performed so far, that solar dynamics will play a role in large LEO space stations.

10.4 SECONDARY POWER SYSTEMS: BATTERIES

Batteries have been used extensively for the secondary power system, providing power during periods when the primary one is not available. As a back-up for a solar array this means that the batteries must provide power during eclipses, and that the array must recharge the batteries in sunlight.

In GEO operations, eclipses only occur during the two equinoctial periods producing eclipse seasons for the spacecraft. These last about 45 days at each equinox. Initially they are short (~minutes), but lengthen to a maximum of 1.2 h before decreasing again. The total of ~90 eclipses, thus, occur irregularly with significant periods of time when no battery operation is required. With more than 22 h of sunlight available in each orbit, a trickle charge solution is possible.

In LEO, on the other hand, the spacecraft may be in eclipse and thus require battery power for 40% of each orbit. Although the precise duration will depend on orbit inclination, it is fairly regular, and the eclipse cycle results in typically 5000 to 6000 charge/discharge cycles of the battery per year. This results in the array-power sizing needing to be nearly twice the nominal load requirement (see Section 10.6).

In summary LEO operations require a large number of low-depth discharges, whereas in GEO a few deep discharges suffice. This inevitably influences battery type, resulting in the present trend of using nickel–cadmium (Ni–Cd) or silver–zinc (Ag–Zn) cells for LEO operation and nickel–hydrogen ($Ni–H_2$) cells for GEO operations. Cell cycle life, specific weight (kW h/kg) and volume (kW h/m^3) all influence the acceptability of a particular battery technology. However, work on more exotic materials, for example, $Li–SO_2$, is continuing [13] and alternative technologies continue to be implemented on spacecraft (see e.g. the annual Goddard Space Flight Center (GSFC) battery workshop proceedings [14]). One of the more recently adopted technologies is the use of a $Li–SO_2$ battery to provide power to the Huygens probe, after separation from the Cassini Saturn orbiter, an event scheduled to occur in 2004. For this rather specialized mission, the probe is in hibernation for 7 years. The battery is then required to provide power during a low power coast for 22 h, and then a high-power load for 2.5 h during descent. For the final 30 min of this period the probe operates from the surface of Titan. For this, the overall battery contains five individual battery units. Each battery consists of two modules of 13 $Li–SO_2$ cells in series. Each cell has a capacity of 7.5 A-h. Table 10.6 summarizes the performance characteristics of a number of cell technologies. Table 10.7 provides specific data for the $Ni–H_2$ batteries for the HST and Intelsat VII.

The detailed electrochemistry of batteries is covered in References [15] and [16]. The main function of battery operation, which is of importance to spacecraft design, is the way in which the reliability and charge efficiency are related to charge control. Parameters of critical importance are the charge/discharge rate, the depth of discharge (DOD), the extent of overcharging and the thermal sensitivity to each of these parameters. Figure 10.15 summarizes some available data on Ni–Cd batteries. A further feature not indicated

Table 10.6 Performance of battery technologies for space use [14]

Type	Specific energy (W h/kg)
Ni–Cd	39
$Ni–H_2$	52
Ag–Zn	60
Ni–MH	60
Li–Ion	80
$Li–TiS_2$	125
Na–S	150

Table 10.7 Hubble space telescope and Intelsat VII $Ni–H_2$ battery summary

Parameter	HST	Intelsat VII
Specific energy (W h/kg)	57.14	61.26
Capacity (A h)	96	91.5
Cell dimensions:		
Diameter (cm)	9.03	8.89
Length (cm)	23.62	23.67
Terminal/terminal (cm)	24.66	29.67
Cell mass (kg)	2.1	1.867

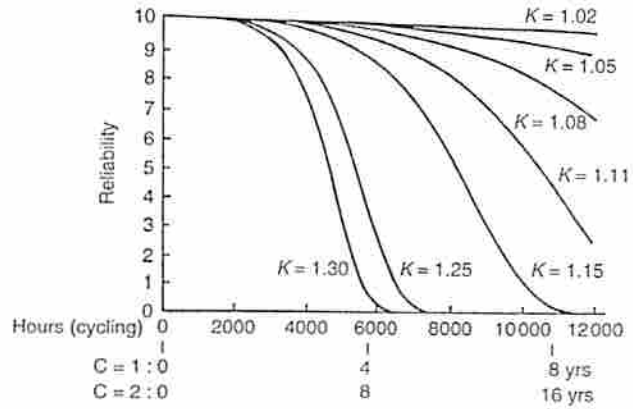

Figure 10.15 Ni–Cd cell reliability as a function of overcharge factor. Hours cycling is related to operation for two cases: $c = 1$, charge rate is battery capacity $\frac{1}{20}$ A/A h; $c = 2$, charge rate is battery capacity $\frac{1}{10}$ A/A h [17] (Reproduced by permission of European Space Agency and P. Montalenti)

in these graphs is the changing performance of a battery after cycling, specifically the change in voltage–current characteristics. The predominant effect is that the charge control system must be flexible if long missions are to be successfully executed. One other notable feature of battery ageing is the effect of hysteresis on the battery capacity. Figure 10.16 demonstrates the loss of this charge capacity over several cycles. It has been noted that if a battery is completely discharged, then capacity may be regained. Whilst this process may result in reverse polarization problems, battery reconditioning before an eclipse season is regularly used for GEO spacecraft. For a given reliability, $Ni–H_2$ batteries may be operated at a greater DOD compared with a Ni–Cd battery, thus requiring for the $Ni–H_2$ a lower installed capacity. As an approximation, for a given number of cycles, a $Ni–H_2$ will be capable of operating at an extra 15% DOD above what is safe to operate a Ni–Cd battery.

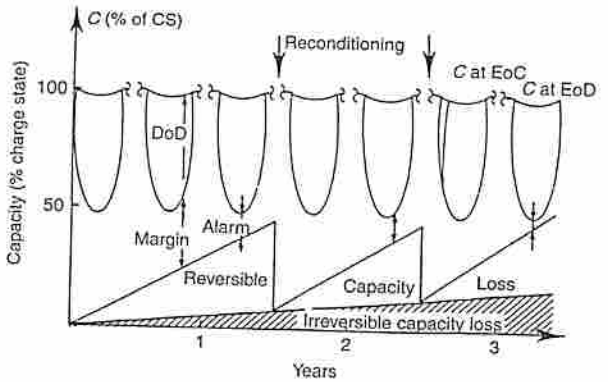

Figure 10.16 Battery reconditioning via complete discharge to improve battery capacity. Both reversible and irreversible capacity loss occurs [17] (Reproduced by permission of European Space Agency and P. Montalenti)

10.5 POWER MANAGEMENT, DISTRIBUTION AND CONTROL

The basic features of power control were outlined in Section 10.2. A key aspect of the power management system is that it must be designed to operate with both a primary and a secondary power system whose characteristics are changing with time as outlined in the previous sections. Several philosophies for power management are outlined in Figure 10.17.

The *electrical 'bus'* may be required to provide a variety of voltages to meet the needs of the various equipment. Generally within Europe, the trend has been to have a regulated dc power bus, typically at 28 or 50 V. For example, the bus of the second generation Meteosat system has a bus voltage of $28.2\,V \pm 1\%$, and for Artemis it is $42.5 \pm 0.5\,V$. Both of these satellites were designed in Europe. In contrast, US spacecraft generally use unregulated buses; for example, the NASA standard for unmanned spacecraft provides a voltage in the range 21 to 35 V dc. Present spacecraft are being designed with higher bus voltages (~150 V) to reduce resistive losses and harness mass. For both regulated and unregulated systems, dc–dc converters are required to provide the variety of voltages needed; this conversion frequently takes place at equipment level rather than centrally.

An ac bus is sometimes used to augment the dc one. The hybrid system can provide mass savings due to both the simplicity of conversion from ac to a variety of dc levels, and also the fact that it is possible to run the power distribution harness at higher voltages if an ac supply is used. Indeed it has been noted [18], that the equivalent wiring cross-section is six times smaller for a three-phase ac network than for a dc one. An ac distribution is mainly applicable to high-power spacecraft and where a large number of dc voltages are required at equipment level. The voltages in ac buses generally have a square waveform, an example being Hipparcos. A notable exception to this is on the Shuttle Space-lab, where the ac bus is more sophisticated, providing a three-phase sinusoidal voltage at 400 Hz.

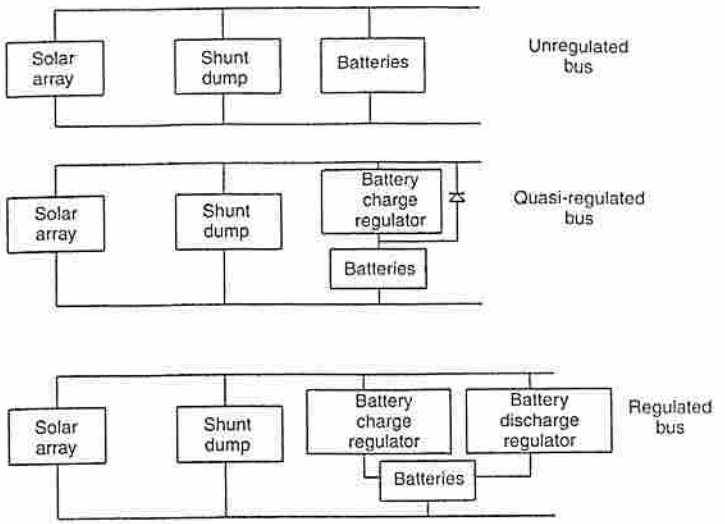

Figure 10.17 Schematic bus concepts

As noted above, the bus can be either regulated or unregulated; in some circumstances it can be quasi-regulated. The fully regulated bus provides voltage regulation during both normal sunlight operation (battery charge cycle) and during an eclipse (discharge cycle). With quasi-regulation, the regulation occurs only during sunlight operation.

The primary units

The main units used in a power system are described below for a typical configuration used on European communications spacecraft. The terminology may differ slightly for US spacecraft. Figure 10.18 shows the overall power system layout.

- *Array regulator*. As the power available from an array varies during a mission, or the power demanded by the payload varies, it is possible to switch in or out segments of the solar array. Switching out is achieved by grounding the individual segments in the shunt dump module. The array itself can be structured into various modules, sometimes called *solar power assemblies* (SPA). The regulation of power output from the array bus is typically achieved by using either a pulse-width modulation scheme, or a sequential switching-shunt regulation, known as S^3R [19]. A considerable number of satellites have used this latter approach. The voltage sensing that is used to control the shunt dump module is termed the *mode control unit* (MCU). An additional strategy used on some spacecraft is maximum power-point tracking. As can be seen from Figure 10.5, the power output from an individual cell shows a distinct maximum. Maximum power-point trackers control the operating point of a string of cells by varying the voltage at which the string operates. As an example [20] of a solar array regulator, the unit on the Artemis satellite, which has a

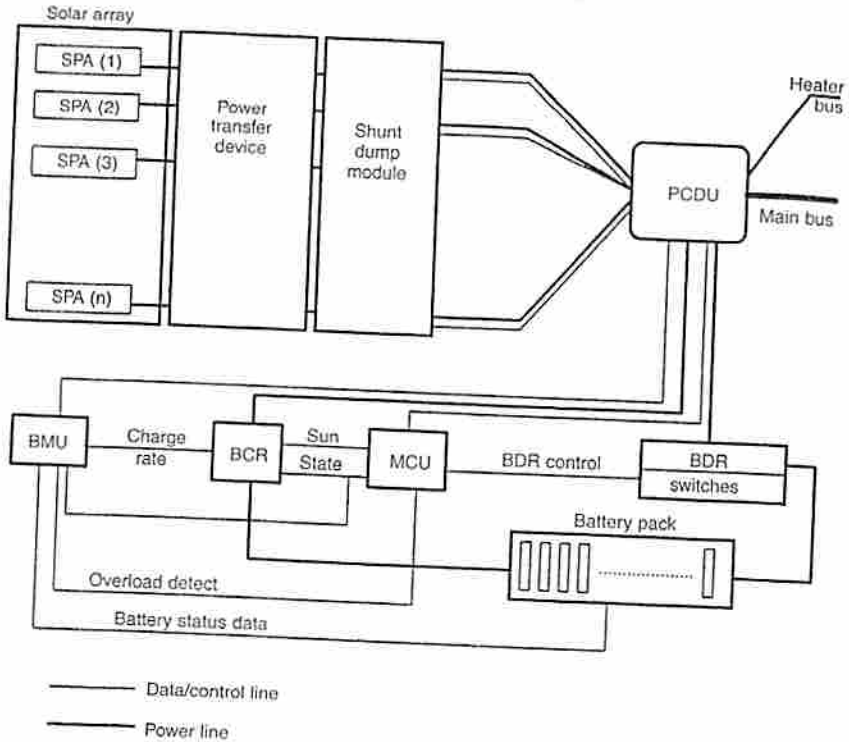

Figure 10.18 Power system layout

sunlight load of 3.3 kW and an eclipse load of 2 kW, provides shunt regulation. This regulator has a mass of 6.5 kg and dissipates 117 W at a nominal load of 2.65 kW. During eclipse operations the regulator requires 18 W.

- *Battery control.* Three units are typically associated with battery control. These are the *battery management unit* (BMU), the *battery charge regulator* (BCR) and the *battery discharge regulator* (BDR). The BMU's functions are to monitor the battery's temperature and voltage as well as individual cell voltages, pressures and temperatures. It is the interface between the power subsystem and the data-handling subsystem, and also provides control inputs to the charge regulation of the batteries, carried out by the BCR. The principal function of the BCR is to provide a constant current charge of the battery during sunlight operation, whilst that of the BDR is to supply a constant current to the spacecraft bus during eclipse operation. Control of this current is derived from the MCU, typically with further protection from the BMU. Whilst the charge/discharge rate of the battery may be controlled in a fairly simple manner through current regulation, the monitoring of the state of charge in a battery is more complex. The principal methods that may be used to sense charge-state are cell voltage, cell temperature, or cell pressure. It should be noted that the level of full charge noted by each of these methods results in a different level of overcharging. Pressure and temperature sensing results in overcharging by 20 to 30%, whereas voltage sensing may indicate 10 to 20% overcharge. A principal problem with voltage sensing arises because of the voltage–charge–temperature characteristics that may cause significant errors in determining the state of charge of the battery. Again taking the Artemis spacecraft as an example, the overall battery control unit has a mass of 25.5 kg. In sunlight, the power required to operate this is 63.5 W and in eclipse, 282 W. The efficiency of the BDR is 89%, and the BCR is 91%.
- *Power control and distribution unit (PCDU).* This unit provides monitoring and protection for the bus current. Protection is normally achieved either by current limiting or by fusing, the latter generally requiring a redundant path to be switched into operation, normally by command from ground-control.
- *Power conversion unit (PCU).* This unit supplies the individual voltage/current characteristics required for loads. The typical low voltage outputs (e.g. ±15 V and 5 V) will be regulated using solid-state switches that are pulse-width modulated. This unit must also be able to cope with transient protection for over- and under-voltage and in-rush current limiting when units are switched on or off.

10.6 POWER BUDGET

The foregoing sections have outlined the principles of the technology behind a power system for use on a spacecraft system. In this section the methodology used to provide the size of a power system is outlined. It is noteworthy that the power subsystem is often the most massive.

10.6.1 Mission specific design issues

The starting point for any power system is in the definition of spacecraft electrical loads. In general these will not be constant throughout the mission, or even throughout a single orbit. The initial analysis must therefore take into account the mission profile and hence the power demand. The three critical issues that need be considered are the orbit parameters, the nature of the mission (communications, science, or other) and the mission duration.

The *orbit selection* has a major influence upon the radiation environment experienced, and hence the degradation anticipated in any solar array-based solution. Further, the orbit will define the duration of eclipse periods (see Section 5.3.2 of Chapter 5), which together with the number of eclipses anticipated, will define battery requirements and the degradation that might be expected to occur during the mission. Clearly in deep-space missions an investigation of the most appropriate technology for the primary power source will be influenced by the orbit.

The *nature of the mission* will have significant impact on the type of loads expected. Thus for a communications satellite, independently of the orbit specification, it can be anticipated that the primary payload will be required at all times. Further, the power demand in eclipse may well exceed that in sunlight, owing to the need both to operate the

payload and to meet the additional burden from active, or power augmented elements, in the Thermal Control System (TCS). Navigation and broadcast satellites will have similar requirements to these. In contrast, a remote sensing spacecraft during eclipse may well not require the whole payload to be operational, particularly if there are passive optical instruments. For such satellites, there may be a very great range of power demands owing to the mission requirements, especially if there are active microwave instruments. These instruments may operate for only limited portions of the orbit, perhaps when communication of data to a ground station is available; this can provide a very high peak load for the power system. Scientific satellites may have very specific payload operational requirements, with additional complexity being provided by the need to download scientific data only when the vehicle is within sight of a ground station. Deep-space missions will inevitably face the temperature extremes that may require additional power for environmental control if the spacecraft either goes very close to or very far from the Sun.

The *mission duration* will provide a major influence on the degradation of the power system. The two most significant influences are

1. The total radiation dose expected which may determine, for a satellite carrying a solar array, the amount of shielding required, and hence influence the specific mass of the power system.
2. The number of eclipse cycles, which will influence the system reliability and its degradation. Solar cell failure through open-circuit losses will clearly increase with increased number of thermal cycles, driven by the entry to and from eclipse. Battery degradation will progress with number of eclipse cycles; indeed for any given technology there is only a maximum number of charge/discharge cycles that a battery can sustain before failure, as shown in Figure 10.16.

10.6.2 Power budget evaluation

The format of a typical power budget is shown in Table 10.8. In this each of the subsystems are identified, with, in this example, power shown simply in terms of eclipse and sunlight loads and peak loads. It is notable that the power subsystem itself also places a load on the spacecraft.

The method adopted for deriving suitable values to insert in this table is as follows: Suppose data is available for each subsystem. Initially such data will exclude the power subsystem. For each subsystem, data must be provided for both the sunlit orbit phase, having, say an average value of P_{sun} and the eclipse phase having an average value of $P_{eclipse}$. Since the satellite must be provided with power throughout the mission, this specifies the EOL requirement.

In reality this approach is highly simplified, since there will be specific events that may place a high transient load on the power system. One such event is the firing of a pyrotechnic device followed by the actuation of some form of deployment mechanism. As an example, the firing of a pyrotechnic release, followed by the deployment of a boom on the Ulysses spacecraft, provided a transient load of nearly two thirds of the total available power from the RTG at the BOL.

In the principal operational phase of a mission, generally not all the spacecraft equipment will be operating at one time. As a result the potential power demand, identified by summing all the spacecraft loads, will never be a realistic value for the peak demand load.

Table 10.8 Typical structure of a power budget

Subsystem	Peak power	Sunlight power P_{sun}	Eclipse power $P_{eclipse}$	Intelsat VIIa (%)	Average GEO comms. satellite (%)
AOCS				5.0	3.6
Power				10.4	11.2
Thermal control				4.9	6.4
Comms.				n/a	n/a
Data handling				0.6	1.6
Payload				79.1	77.2
Average total power				100	100

Indeed in many cases it will be found that such a summation exceeds the total power availability from the power bus. One subsystem that has widely varying requirements during a mission is the thermal system. This subsystem must meet both a hot and cold case, which may require very different levels of heater input. Again taking the Ulysses mission as an example, the 'hot' case heater power (8.7 W) was only one third that of the 'cold' case heater load (24.7 W).

For telecommunications spacecraft operating in GEO there is a fairly well-defined power profile between subsystems. Increasingly, as noted in Chapter 6, electric propulsion is being used on such missions for station keeping control, which results in an increase in the power required for the propulsion subsystem. Power for propulsion in Table 10.8 is included in the AOCS subsystem in the power profile. This is shown as a percentage for each of the subsystems for recently launched GEO communications satellites. The specific profile for Intelsat VIIa is also shown.

10.6.3 Power system sizing

A simplified block diagram for the power system is shown in Figure 10.19, in which the efficiencies of various components are also identified. Representative values for the efficiencies may be found in Sections 10.3, 10.4 and 10.5.

Consider a general case for sizing a power system. Assuming that the orbit period is τ, with the time spent in sunlight τ_{sun}, and the time spent in eclipse $\tau_{eclipse}$, then the power required from the array to meet the eclipse load is clearly given by P_{charge}, where

$$P_{charge}\tau_{sun} = \frac{1}{\eta}P_{eclipse}\tau_{eclipse} \tag{10.5}$$

and η is the product of the efficiency terms shown in Figure 10.19,

$$\eta = \eta_{BDR}\eta_{BCR}\eta_{AR}$$

The total power required to be available from the array is thus approximately given by

$$P_{array} = P_{sun} + P_{charge} \tag{10.6}$$

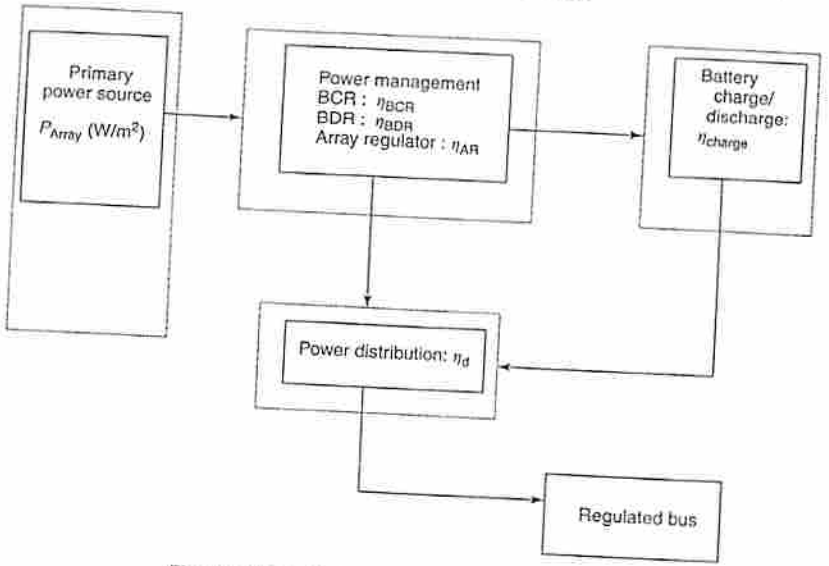

Figure 10.19 Definition of system efficiencies

In the limit, if all the efficiencies are equal to unity, it is apparent from equations (10.5) and (10.6) that if the eclipse power demand is the same as that in sunlight then the array power is simply given by

$$P_{array} = P_{sun}\left(\frac{\tau}{\tau_{sun}}\right) \tag{10.7}$$

Thus for LEO orbits where the fraction of the orbit in eclipse is large, typically of the order of 30 min out of 90 min, the array needs to be oversized relative to the sunlight provision by a factor τ/τ_{sun} of approximately 1.5. Hence, in this approximate scenario, the array power in LEO is required to be 50% in excess of the bus load. This may be contrasted with the GEO case where a maximum eclipse duration of ~70 min in the 24-hour orbit arises. In this case the 'oversizing' of the array amounts to only 5%. This feature clearly has significant influence over the design of a solar array.

If the orbit period is τ (hours), the battery-stored energy will be given approximately by E_B (W-hrs)

$$E_B = P_{eclipse}(\tau - \tau_{sun})/(\eta_{charge} DOD) \tag{10.8}$$

where the DOD is the depth of discharge of the battery. The battery mass can be estimated by dividing the stored energy (W-hrs) by the energy density (W-hrs/kg) for the chosen battery technology. For example, for Ni–Cd the energy density is approximately 30 to 40 W-hrs/kg.

In any particular case, the individual loads that will be switched in and out need to be considered. We can then modify equation (10.5) to obtain the total energy required from the array. This may be written in the form ε_{array} where

$$\varepsilon_{array} = P_{array}\tau_{sun} = \frac{1}{\eta_{sun}}\left(\sum_{i=1}^{k} P_i t_i\right) + \frac{1}{\eta_{ecl}}\left(\sum_{i=k+1}^{n} P_i t_i\right) \tag{10.9}$$

in which the $P_i, i = 1, \ldots, n$, gives the typical power profile for payload and subsystem operation throughout the orbit. A typical profile may be as illustrated in Figure 10.20. The battery charge requirement during sunlight is explicitly excluded from this profile, since the eclipse profile (second term in equation 10.9) is equivalent to the battery charge energy (see equation 10.5). For the purposes of a first estimate of the array size, the efficiency factors have typical values of η_{sun}~0.8, from array to loads, and η_{ecl}~0.6, from batteries to loads.

In terms of calculating the array size, allowance needs to be made for any pointing-angle offset of the array relative to the sun line. This results in the array area being given by A_{array} where

$$A_{array} = P_{array}/(S\cos\delta\theta\,\eta_{cell}\eta_{packing}(1 - D)) \tag{10.10}$$

Here S is the solar flux (~1400 W/m² in a near-Earth orbit); $\delta\theta$ is the array pointing error with respect to the Sun, which will typically be of order 1°, but is highly dependent on the mission; η_{cell} is the solar cell efficiency; $\eta_{packing}$ is the cell packing efficiency that is typically 0.90; D is the array degradation factor over the spacecraft lifetime, which may be calculated in the manner described in Section 10.3.1.

In a specific design, the sizing of the array given by the equivalent of equation (10.7) will be modified to include specific mission profiles for 'hot' and 'cold' cases. These differing cases arise during the year, as a result of variation in solar insolation, which will influence the array temperature (see Chapter 11); this variation occurs due to the influence of the angle between the orbit plane and the ecliptic. As a result, the final EOL array and battery capacity can be specified. To define the BOL characteristics, loss factors due to radiation damage, micrometeorite damage and battery hysteresis losses must included. Thus this process evidently requires the array and battery capacity to be oversized initially to meet the EOL power demands. Typically these loss factors may rise to 25% of the

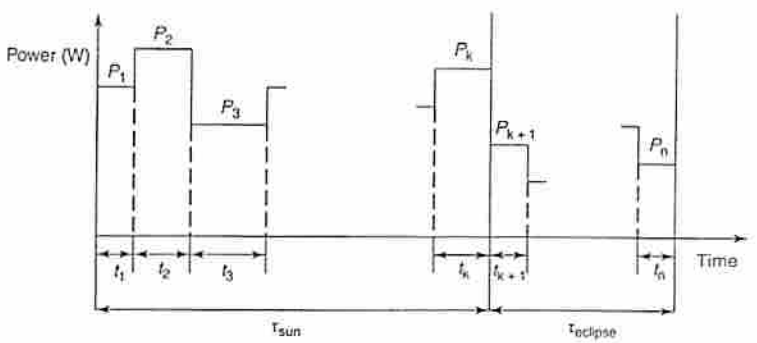

Figure 10.20 Approximate power profile for payload and subsystem operation throughout the orbit

initial provision, although this figure is highly dependent upon both mission duration and the type of orbit, with Highly Elliptical Orbits (HEOs) being particularly affected by radiation damage.

REFERENCES

[1] *SPS Concept Development and Evaluation Programme Reference System Report* (1978) US DOE and NASA DOE/ER 0023.
[2] Angrist, S. W. (1982) *Direct Energy Conversion*, Allyn and Bacon, New York.
[3] Bennett, G. (1995) Summary of the US Use of Space Nuclear Power, ESA SP 369, 163–169.
[4] Sheibley, D. W. (1983) Regenerative H_2-O_2 Fuel Cell—Electrolyser Systems for Orbital Energy Storage, NASA CP-2331, 23–38.
[5] Rauschenbach, H. S. (1980) *Solar Cell Array Design Handbook*, Van Nostrand Reinhold, New York.
[6] Taylor, H., Simpson, A. F. and Dollery, A. A. (1984) CMX-50: A New Ultra-thin Solar Cell Cover for Lightweight Arrays, ESA SP-173, 211–214.
[7] Mawira, D. (1982) Advanced Rigid Array, ESA SP-173, 9–14.
[8] van Hassel, R. (1999) Achievements and Prospects for ARA Mark III Solar Array Product Range, IAF-99-R.2.07.
[9] Knorr, W., Theurer, G. and Schwartz, M. (1995) A Regenerative Fuel Cell System for a Lunar Rover, ESA SP-369, 21–26.
[10] Bockris, J. O.'M. and Srinivason, S. (1969) *Fuel Cells and Their Electrochemistry*, McGraw-Hill, New York.
[11] Terrill, W. and Haley, V. (1986) Thermoelectric Converter for SP-100, *21st IECEC*, 1950–1955.
[12] *Solar Dynamic Power System Development for Space Station Freedom*, NASA RP1310 (1993).
[13] Dudley, G. J. (1998) Lithium Ion Batteries for Space, ESA SP-416, 17–24.
[14] Halpert, G. and Surampudi, S. (1993) Advanced Energy Storage for Space Applications, NASA CP 3254, 91–110.
[15] NASA RP 1052 (1979).
[16] NASA SP 172 (1968).
[17] Montalenti, P. (1977) Software/Hardware Interface in Control and Protection of Space Batteries, ESA SP-126, 271–278.
[18] Eggers, G. (1985) AC Buses for LEO—A Viable Alternative, ESA SP-230, 17.
[19] Knorr, W. (1998) Power System for 2nd Generation Meteosat, ESA SP-416, 11–16.
[20] ESA SP-369 4th European Space Power Conference (1995).

11 THERMAL CONTROL OF SPACECRAFT

Chris J. Savage

Head of Thermal and Environmental Control Section, European Space Research and Technology Centre, European Space Agency

11.1 INTRODUCTION

Spacecraft thermal control—that is the control of spacecraft equipment and structural temperatures—is required for two main reasons: (1) electronic and mechanical equipment usually operate efficiently and reliably only within relatively narrow temperature ranges and (2) most materials have non-zero coefficients of thermal expansion and hence temperature changes imply thermal distortion.

Spacecraft equipment is designed to operate most effectively at or around room temperature. The main reason for this is that most of the components used in spacecraft equipment, whether electronic or mechanical, were originally designed for terrestrial use. It is also much easier and cheaper to perform equipment development and, eventually, qualification and flight acceptance testing at room temperature. Typically, operating electronic equipment requires to be maintained in a temperature range between about −15 °C and +50 °C, rechargeable batteries between about 0 °C and +20 °C and mechanisms (solar array drives, momentum wheels, gyroscopes etc.) between about 0 °C and +50 °C. There are, of course, exceptions to this—for example, some detectors within astronomical telescopes that need to be cooled to very low temperatures.

Many spacecraft payloads require very high structural stability, and therefore thermally induced distortion must be minimized or strictly controlled. For example, the search for ever-higher resolution from space-based telescopes means that temperature stability of a fraction of one degree is often required within telescope systems several metres in size.

Heat is generated both within the spacecraft and by the environment. Components producing heat include rocket motors, electronic devices and batteries. Initial ascent heating effects are minimized by the launch vehicle's nose fairings or, in the case of launch by the Space Shuttle, by the cargo-bay doors. Heat from the space environment is largely the result of solar radiation. Heat is lost from the spacecraft by radiation, mainly to deep space. The balance between heat gained and heat lost will determine the spacecraft temperatures.

Spacecraft Systems Engineering (Third Edition). Edited by P. W. Fortescue, J. P. W. Stark and G. G. Swinerd